

NeCl₂ and ArCl₂: Transition from Direct Vibrational Predissociation to Intramolecular Vibrational Relaxation and Electronic Nonadiabatic Effects[†]

Craig R. Bieler[‡] and Kenneth C. Janda

Department of Chemistry, University of California, Irvine, California 92697

Ramón Hernández-Lamonedá

Centro de Investigaciones Químicas, Universidad Autónoma de Morelos, Avenida Universidad 1001, Cuernavaca, Morelos 62210, Mexico

Octavio Roncero*

Instituto de Física Fundamental, CSIC, Serrano 123, 28006 Madrid, Spain

Received: July 7, 2009; Revised Manuscript Received: August 7, 2009

Pump–probe results are reported for NeCl₂ excited to the Cl₂ B state, undergoing vibrational predissociation, and then probed via E ← B transitions. Intensities, lifetimes and product vibrational branching ratios are reported for $16 \leq v' \leq 19$ Cl₂ stretching quanta. The intensity of the signal rapidly decreases above $v' = 17$. Detailed wave packet calculations of the vibrational predissociation dynamics are performed to determine if the experimental results can be explained by the onset of IVR dynamics. The calculations and the experiment are in close accord for low vibrational levels. For higher levels, some, but not all, of the loss of experimental signal can be attributed to IVR. To test whether electronic relaxation dynamics are important for NeCl₂ and ArCl₂, excited state potential surfaces that incorporate spin orbit coupling effects are calculated. These surfaces are then used in a wave packet calculation that includes both vibrational predissociation and electronic predissociation dynamics. The results show that electronic predissociation is important for ArCl₂ levels above $v' = 12$. For NeCl₂ the calculation suggests that the onset of electronic predissociation should occur for levels as low as $v' = 13$ but may not contribute markedly to the observed loss of signal above $v' = 17$. Suggestions are made for further studies of this puzzling problem.

I. Introduction

The noble gas–halogen dimers have provided a rich model system for investigating van der Waals interactions and molecular dynamics. The fact that the homonuclear dihalogen species have two nearly equally deep wells, one linear and one perpendicular to the halogen bond, caused years of confusion.^{1–3} This was mainly due to the fact that the linear isomers are difficult to observe by laser excited fluorescence since there is no comparable well for the excited state, and thus the visible absorption spectra for the linear isomers are nearly continuous and difficult to observe.^{4–7} In contrast, the spectra for the “T” shaped isomers exhibit a sharp rotational structure that is relatively easy to observe and analyze. Once it was clear that both isomers exist,^{7–14} it was reasonably straightforward to analyze the details of the half-collision vibrational dynamics: mostly direct dissociation for the linear isomers and direct vibrational predissociation for the “T” shaped isomers when the $\Delta v = -1$ relaxation channel is open and multistep intramolecular vibrational relaxation (IVR) when the $\Delta v = -1$ relaxation channel is closed. In the case of IVR, the dynamics are so sensitive to the details of the potential that it is still not possible to obtain direct agreement between experiment and theory.¹⁵

Another issue for which experiment and theory have yet to converge is the competition between vibrational dynamics and electronic dynamics. That such competition exists was first realized for the Ar–I₂ molecule. Oscillations in the laser excited fluorescence intensity as a function of vibrational level were attributed to the competition between vibrational and electronic predissociation in the electronic B state.¹⁶ (Here, as usual, we apply the electronic state label for the halogen moiety to the van der Waals complex as well.) Also, the failure to observe Ar_nI₂ clusters with $n > 3$ was attributed to rapid electronic predissociation.¹⁷

Many theoretical studies have been devoted to this process, without complete success, as has been recently reviewed.¹⁸ Burke and Klemperer¹⁹ measured the vibrational predissociation (VP)/electronic predissociation (EP) relative efficiency for $v = 16–23$ and concluded that the observed oscillations are due to EP, while the VP rate may increase monotonically with v . The oscillations of the EP rate were confirmed theoretically using a time dependent Golden rule treatment for the electronic predissociation.²⁰ It was found, however, that the VP rate oscillates more drastically than EP due to the appearance of IVR in ArI₂ in the sparse-intermediate regime.²¹ The occurrence of the statistical IVR regime necessary to explain a smooth variation of the VP rate with v was further analyzed for ArCl₂,²² concluding that it was only possible after rotational averaging. Recent calculations^{23,24} of the competition between VP and EP dynamics found that even when the EP rate presents some weak oscillations, those associated with VP are more intense. Thus

[†] Part of the “Benoît Soep Festschrift”.

* Corresponding author: e-mail Oroncero@imaff.cfmac.csic.es.

[‡] Permanent address: Department of Chemistry, Albion College, Albion, MI.

the details of the competition between vibrational and electronic predissociation in ArI₂ remain an open problem. Total decay rates have only been measured for $\nu = 18$ and 21.²⁵ More data would be very helpful.

For other noble gas–halogen species, even less is known. The lowest bromine stretching vibrational levels of the noble gas–Br₂ B state species have yet to be observed. This may be due to a curve crossing between the bromine B and C states at the energy of $\nu' = 4$ of the B state. For the noble gas–Cl₂ species, the results are slightly more complex. No laser excited fluorescence or pump–probe signals have been observed for the Ar–Cl₂, B state, vibrational levels $\nu' > 12$.²⁶ Again, this is thought to be due to a curve crossing between the chlorine B and C states near the energy of the 12th chlorine B state stretching vibration. Also, this is the first vibrational level whose energy is above the asymptote for dissociation to two ground state chlorine atoms. In contrast, pump–probe spectra are observed for higher vibrational levels of HeCl₂^{27,28} and NeCl₂.^{29,30} For these two species, as for ArI₂, electronic predissociation is slow enough that vibrational predissociation remains competitive over a broad range of vibrational levels. For HeCl₂, the signals due to vibrational predissociation become unobservable above $\nu' = 24$.²⁸ For NeCl₂, as reported below, the signals due to vibrational predissociation become quite weak above $\nu' = 16$. Unlike the oscillating intensities observed for ArI₂, the signals for the Cl₂ complexes remain quite strong, and then disappear fairly quickly with increasing vibrational level. It so happens that for each of the noble gas–Cl₂ dimers, with Ng = He, Ne, and Ar, the electronic relaxation rate appears to increase abruptly for vibrational levels near the closing of the $\Delta\nu = -1$ vibrational predissociation channel. This led us to speculate that the onset of electronic predissociation is coupled to the onset of IVR dynamics.³¹

For the heavier noble gas species Kr and Xe–Cl₂^{32,33} weak pump–probe signals due to vibrational predissociation were observed for only a few vibrational levels:³² $\nu' = 8$ –11 for Kr–Cl₂ and $\nu' = 10$ –11 for Xe–Cl₂.³² In both cases, the $\Delta\nu' = -2$ channel is the lowest energy transfer dissociation pathway. In these cases, the highest vibrational level observed is even lower than for Ar–Cl₂, probably due to the fact that the heavier noble gas atoms enhance the coupling between the B and C states, and perhaps also indicating that the reaction $\text{KrCl}_2 \rightarrow \text{KrCl} + \text{Cl}$ is participating to lower the probability of probing Cl₂. However, this does not explain the lack of vibrational predissociation signals for the lower vibrational states. One possible explanation for this phenomenon is that the vibrational predissociation rate for these lower vibrational levels is so slow that electronic nonadiabatic transitions are faster than vibrational predissociation even without a nearby curve crossing.

One reason a theoretical treatment for the competition between electronic and vibrational predissociation is difficult is that the relevant potential energy surfaces for the noble gas–halogen excited states are difficult to calculate and therefore still poorly characterized. In particular, it is not possible to achieve the correct angular momentum symmetry for the states without explicitly including spin-orbit coupling. For the B states, a common practice is to take the simple average of the two lowest energy states that correlate with the triplet electronic symmetry.³⁴ This approximation might work well in some cases, particularly for vertical excitation energies and sampling restricted regions of the potential energy surfaces. However, this approximation is clearly insufficient if one wants a global description of the interactions. In particular, it will fail to reproduce the correct asymptotic dissociation limits of the

halogen diatomic states, which is crucial for obtaining even a qualitative understanding of the properties of highly excited vibrational states. For calculations including spin–orbit effects, the analysis becomes very complicated due to the numerous spin–orbit states that appear when approaching the dissociation limit of the diatomic. This in turn leads to several curve crossings all of which in principle can be of relevance. In this sense it is worth mentioning the photodissociation study by Asano and Yabushita³⁵ where they show that out of several nonadiabatic mechanisms only those of a given type (Rosen–Zener–Demkov) turn out to be relevant for the photodissociation process.

Recently, we reported three-dimensional potential energy surface calculations, explicitly including spin–orbit coupling, for the valence excited states of Ne–Cl₂.³¹ It was found that a ³Π_{2g} state crosses the B ³Π₀ for Cl–Cl distances of about 6 bohr. Furthermore, the coupling of the two states is strongly modulated by the position of the Ne atom. In particular, for the “T” shaped geometry, even though the two states belong to the same symmetry, they are not coupled. The coupling increases noticeably with bending angle, so that zero-point motions may sample the coupling region. We postulated that this angle dependent coupling may be the explanation for the coupling between IVR dynamics and the electronic relaxation rate.

In this paper we pursue three goals. First, we report data to more accurately characterize the details of the competition between vibrational and electronic predissociation for the Ne–Cl₂ dimer. Second, we report *ab initio* calculations on the valence-excited states of Ne– and Ar–Cl₂ that incorporate spin–orbit coupling. Third, we report wave packet calculations of the vibrational and electronic dynamics for the two systems on the newly available potential energy surfaces and couplings. The new theory is qualitatively consistent with the experimental data for ArCl₂ but does not achieve comparable agreement for NeCl₂. We end by discussing possible next steps for solving this long-standing problem.

II. Experimental Section

The experiments reported here are very similar to those reported in a previous study of NeCl₂,³⁰ except that higher vibrational levels were studied. The NeCl₂ molecules are formed in a pulsed supersonic expansion and studied via pump–probe spectroscopy employing two 20 ns pulsed excimer-pumped dye lasers with 0.2 cm^{−1} frequency resolution. The pump and probe pulses are separated by 10 ns at their intersection with the nozzle pulse, 0.5 cm downstream from the nozzle. The pump laser excites the NeCl₂ X, $\nu'' = 0 \rightarrow \text{B}$, ν' transition to the desired ν' level. (ν' is the Cl₂ stretching vibration quantum number in the B electronic state.) During the 10 ns delay before the probe laser pulse the NeCl₂ undergoes vibrational predissociation by losing one or more Cl₂ stretching quanta to break the Ne–Cl₂ bond. The product Cl₂ molecule remains in the electronic B state but has a lower vibrational quantum number. The product Cl₂ state is detected by exciting it to the E electronic state and detecting the resulting fluorescence. The intensities of the pump–probe signals are determined by a variety of factors, including the laser pulse intensity, Franck–Condon factors, saturation, and sample number density. In general, we use published Franck–Condon factors and double resonance intensities to calibrate our signals. For instance, if we know the ratio of the free chlorine excitation to $\nu' = 16$ and 18, we assume the same relative efficiency for NeCl₂.

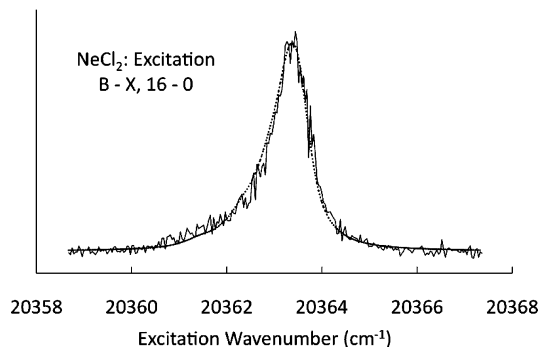


Figure 1. Excitation line shape for the NeCl₂, X → B, $v'' = 0 \rightarrow v' = 16$ transition. Note the excellent signal-to-noise ratio. The dotted line is a fit to the data described in the text that yields an excited state lifetime $\tau = 11$ ps.

III. Experimental Results

An example of an excitation spectrum is shown in Figure 1. This spectrum was obtained by setting the probe laser to detect the Cl₂, B state, $v' = 15$ while the pump laser is tuned over the NeCl₂, X → B, $v'' = 0 \rightarrow v' = 16$ transition. The resolution of the spectrum is limited by the short lifetime of the NeCl₂ B state vibrational level, $\tau = 11$ ps. The lifetime is obtained by convoluting a Lorentzian line shape with the calculated rotational substructure and the laser line width. The rotational substructure is estimated by assuming that the Ne–Cl₂ bond length is unchanged from lower vibrational levels, for which it can be measured, and that the Cl–Cl bond length is unchanged from that of the free molecule in the corresponding vibrational level. The dashed line shown in Figure 1 is the convoluted fit to the data. Similar data were obtained for the levels $v' = 14$ to $v' = 17$. The results are given in Table 1.

An example of a probe spectrum is given in Figure 2. This spectrum was obtained by setting the pump laser on the center of the NeCl₂, X → B, $v'' = 0 \rightarrow v' = 16$ transition shown in Figure 1, and tuning the probe laser over the Cl₂ B → E, $v' = 15 \rightarrow v = 13$ transition. Although the probe spectrum is too congested to extract an unambiguous product rotational state distribution, it is sufficiently resolved to conclude that only levels up to $J = 16$ are populated. This upper limit for J allows us to determine the bond energy for Ne attached to Cl₂, B, $v' = 16$ as described previously.²⁹ The result is D_0 (NeCl₂, B, $v' = 16$) = 54.8 ± 2.2 cm^{−1}. $\Delta v = -2$ probe spectra were also observed by detecting Cl₂, $v' = 14$. From the intensity of these spectra, the $\Delta v = -2:\Delta v = -1$ branching ratio is 0.28. New bond energy and branching ratio data measured in this study are also included in Table 1.

The original goal of this study was to characterize the closing of the $\Delta v = -1$ dissociation channel to investigate if the dynamics change to the intramolecular vibrational relaxation regime, analogous to that observed for ArCl₂,^{15,22,26} NeBr₂,^{36–38} and HeBr₂. To our surprise, however, the spectra for NeCl₂ vibrational levels above $v' = 16$ became significantly less intense. The analogous free Cl₂ double resonance transitions and HeCl₂ pump–probe signals are quite strong for these levels due to favorable Franck–Condon factors.²⁸ We thus suspect that a “dark” relaxation channel, possibly involving a nonadiabatic coupling to another electronic state, is responsible for the disappearance of the pump–probe spectra for these higher vibrational levels. This stimulated the theoretical work reported below.

IV. Theory of Vibrational Predissociation and IVR

The fragmentation dynamics of the excited NeCl₂ molecules were simulated for $11 \leq v' \leq 21$ using an exact wave packet treatment described in detail elsewhere.²² Only a brief summary of the method is provided here. The coordinates for the calculation are r , the Cl–Cl distance, R , the Ne–Cl₂ center of mass separation, and γ , the angle formed by the Ne–Cl₂ and the Cl₂ bonds. The initial “bright” state, ϕ_1 , corresponds to a single Cl₂(B, v') vibrational level with the van der Waals modes in their ground states. These states, denoted by their J , K , and v quantum numbers are calculated variationally in basis sets composed of numerical radial functions multiplied by angular functions composed of Wigner rotation matrices and spherical harmonics. The Cl₂ r coordinate is described by a single $\chi_v(r)$ vibrational function for free Cl₂(B, v').

The dissociation dynamics are followed by expanding the wave packet as

$$\Psi_t^{J,M,K,v} = \sqrt{\frac{2J+1}{8\pi^2}} \sum_{\Omega,v'} D_{M\Omega}^{J*}(\phi, \theta, \chi) \chi_v(r) \Phi_{\Omega,v'}^{J,K,v}(R, \gamma; t) \quad (1)$$

where $D_{M\Omega}^{J*}$ are Wigner rotation matrices relating the body-fixed and space-fixed frames through the ϕ , θ , χ Eulerian angles.

For each initial v' state, 11 vibrational functions, $v' - 7, v' - 6, \dots, v' + 2$, are used in the expansion. The $\Phi_{\Omega,v'}^{J,K,v}(R, \gamma; t)$ coefficients are described in finite grids formed by 256 equidistant points for R over the interval $1 \leq R \leq 18$ Å and 60 Gauss Legendre quadrature points over the interval $0 \leq \gamma \leq \pi/2$. The coefficients are obtained by numerically integrating the corresponding time dependent Schrödinger equation using a Chebyshev propagator,⁴⁰ with 50 fs time step. At each time step the wave packet is multiplied by an absorbing function, $f(R) = \exp[-\alpha(R - R_{\text{abs}})^2]$, with $\alpha = 0.025$ Å^{−2} and $R_{\text{abs}} = 15$ Å. The propagation is performed until about 99% of the probability has been absorbed.

The potential used in this work is taken from ref 30, which was obtained by fitting NeCl₂ data for $v' \leq 12$. An RKR function describes the Cl–Cl bond and an atom–atom Morse potential is used to describe the Ne–Cl₂ interaction.

V. Theoretical Results on Vibrational Predissociation and IVR

The bound state energy and lifetime, $\Delta v = -2/\Delta v = -1$ branching ratios and band intensities were calculated as described above, and the results are presented in Table 1. Given that the potential energy surface used for these calculations was obtained by fitting data only from levels with $v' \leq 12$, calculated results are in remarkably good agreement with the data, except for the relative intensities. We infer that the potential energy surface is sufficiently accurate to characterize the onset of IVR dynamics with increasing vibrational excitation.

Figure 3 shows the calculated excitation line shapes for $v' = 16$ –21. The $v' = 16$ line shape is nearly Lorentzian, which indicates that the dynamics for this and lower vibrational levels are dominated by simple vibrational predissociation. The influence of IVR dark state mixing starts to appear for $v' = 17$ and becomes increasingly evident for larger v' . IVR is extensive enough for $v' = 20$ and 21 so that there is no clear closing of the $\Delta v = -1$ dissociation channel since the excitation spectrum extends over a broad energy range. For $v' = 16$ the spectrum is about 2 cm^{−1} wide, by $v' = 21$ the IVR structure extends over

TABLE 1: Measured and Calculated Properties of the NeCl₂, B State, 11 < ν' < 20

ν'	$D_{0,\text{exp}}$ (cm ⁻¹)	$D_{0,\text{theo}}$ (cm ⁻¹)	τ_{exp} (ps)	τ_{calc} (ps)	$\Delta\nu = -2/-1$ (exp)	$\Delta\nu = -2/-1$ (calc)	intensity ^a (exp)	intensity ^a (calc)
11		-54.4	100 ± 6 ^b	103	0.06	0.05		
14			24 ± 3					
15		-53.7	18 ± 3	15.5		0.16		
16	55 ± 2	-53.4	11 ± 2	7.9	0.28	0.25	1.0	1.0
17	55 ± 2	-53.1	6 ± 1	5.0	0.34	0.35	0.77	0.52
18		-52.7		4.0		0.56	0.25	0.61
19		-52.3		2.6		0.87	0.06	0.45
20		-51.7		1.7		2.0		0.32
21		-51.0		1.2		>10		0.22

^a Band intensity relative to that for $\nu' = 16$. The experimental results are corrected for Franck–Condon factors. ^b From ref 55.

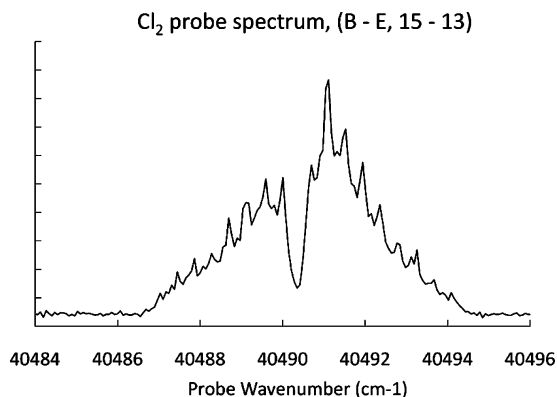


Figure 2. Probe spectrum of the Cl₂, B → E, $\nu' = 15 \rightarrow \nu = 13$ transition, with the pump laser set on the maximum of the spectrum shown in Figure 1. Although the product rotational distribution is not resolved, it is clear that low J products are most heavily weighted, and that the highest observed value of J is 16. This yields a Ne–Cl₂ bond energy of 55 cm⁻¹, as described in the text.

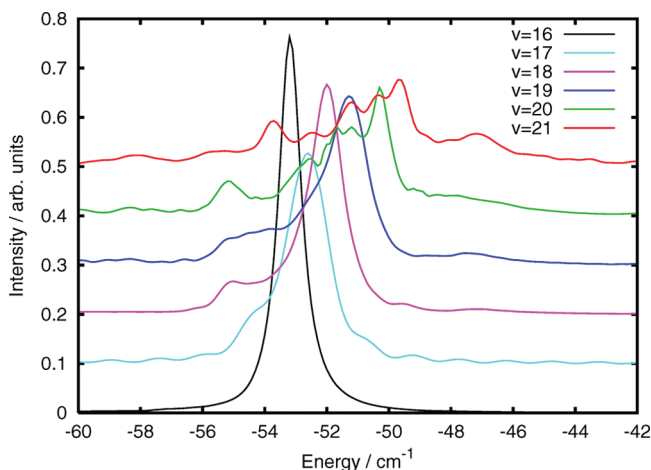


Figure 3. Calculated absorption spectra for different NeCl₂(ν) levels. For $\nu' \geq 16$, the effects of IVR become more evident, resulting in broader, more complicated excitation line shapes. The energy scale is with respect to the initial state dissociation limit.

a 10 cm⁻¹ range. That the structure in the calculated spectra of Figure 3 is due to IVR is further confirmed by the calculated decay curves, which are smooth and single exponential for $\nu' = 16$ but show increasing structure and recurrences for the higher levels.

Although the peak intensity of the calculated absorption spectra decreases with ν' , the effect is not enough to account for the disappearance of the experimental spectra since the signal-to-noise ratio for $\nu' = 16$ is excellent. According to the IVR calculation, the peak excitation intensity for the 20 ← 0 band is 32% that of the 16 ← 0 band. The pump–probe signals

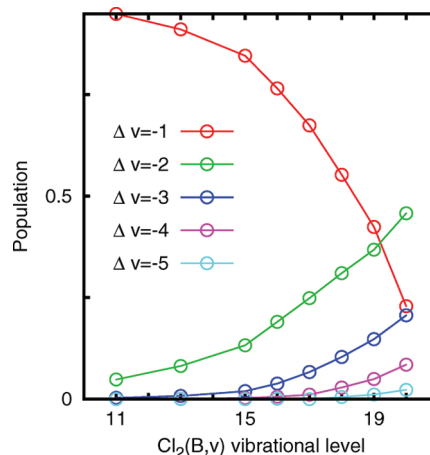


Figure 4. Simulated final vibrational channels of Cl₂(B, $\nu - \Delta\nu$) products after vibrational predissociation of the initial Ne–Cl₂(B, ν) level.

for the 20 ← 0 band would also be weaker due to a broader distribution of vibrational product states, as shown in Figure 4. However, the high signal-to-noise levels of the pump–probe technique would result in good signal levels in the absence of another decay channel.

Of course, the results reported in this section depend on the validity of the assumed potential. The potential accurately reproduces the experimental results in the direct VP regime. However, in the IVR regime the results are much more sensitive to the details of the potential. It would not be too difficult to modify the potential to predict lower intensity levels for the experiment. However, the calculated lifetimes are already shorter than the measured ones for $\nu' = 15$ –17, although the differences are small. For now, we prefer to accept the results for the current potential and investigate whether electronic predissociation may be the reason for the weak signals of higher vibrational levels.

VI. Nature of the Dark Relaxation Channel

The appearance of a new “dark” channel would further reduce the emission intensity from a particular Cl₂(B, ν') final state. The most likely dark channel is electronic predissociation toward a dissociative state of Cl₂. As discussed in the Introduction, such processes have been studied intensively for ArI₂.¹⁸ Recently, it was suggested that EP is probable in the NeCl₂ system due to couplings between the B and the 2g dissociative states of Cl₂ for bent configurations of the dimer.³¹ This suggestion was based on ab initio multireference configuration interaction (MRCI) calculations including relativistic effects. Here we analyze this possibility in more detail and make quantitative calculations of the EP probability. We also extend the results to ArCl₂. To achieve this goal, it was first necessary to calculate potential energy surfaces and electronic coupling for the two molecules.

Next, wave packet calculations were performed to study the relative importance of vibrational and electronic dynamics.

VII. Calculation of Potential Energy Surfaces and Couplings

The accurate calculation of the electronic states of the dihalogens is a challenge for *ab initio* quantum chemistry.^{41,42} In particular, the group of Buenker has shown the slow convergence of spectroscopic properties with respect to both the Gaussian basis and the configuration interaction (CI) expansion. Additionally, one has to include spin–orbit effects even for a qualitative understanding of the excited states, in particular those crucial for the present study. Finally, we want to reproduce the weak intermolecular forces present in both NeCl₂ and ArCl₂ complexes which, as is well-known, requires the use of highly correlated wave functions together with size consistency properties.⁴³ There is no current *ab initio* methodology that can tackle all these challenges simultaneously. Furthermore, the general treatment of excited states and bond dissociation, required in this work, can only be obtained with limited CI techniques, which are not appropriate for the treatment of intermolecular forces. For these reasons we have adopted a mixed approach for the representation of the potential energy surfaces using *ab initio* methodology to gain new insight into the electronic predissociation mechanism together with experimental information to improve our quantitative predictions.

The *ab initio* methodology has been described in our previous study of NeCl₂,³¹ and here we only summarize the main ingredients. We use the relativistic effective core potential (RECP) of chlorine developed by the Stuttgart group,⁴⁴ which provides an efficient way of including spin–orbit effects. The original valence basis has been extended with polarization and diffuse functions to yield the final set 3s3p3d2f1g. For the noble gases we use the correlation consistent AVTZ basis set. The relevant spin–orbit states are obtained by diagonalizing the total Hamiltonian, which consists of the usual electronic part plus the spin–orbit interaction term. The basis for diagonalization is obtained by first optimizing the orbitals in a complete active space (CAS) defined by the valence electrons and orbitals of chlorine together with a state-averaging of nine electronic states close in energy to the spectroscopic states under study. We then perform MRCI calculations to include dynamic electron correlation including the Davidson correction and the valence electrons of the noble gas. The total number of spin–orbit states obtained is 36. All calculations were performed with the MOLPRO2006.1 package.⁴⁵

In Figure 5 we show the B/2g curve crossing for the isolated chlorine molecule. For the B state we employ the RKR potential of Coxon et al.⁴⁶ while for the 2g state two potentials are compared: one coming from the group of Buenker^{41,42} and the other our best *ab initio* result, both shifted in energy so that the asymptotic difference with the B state coincides with the experimental spin–orbit splitting (881 cm^{−1}) between ground and first excited atomic levels. We have kept the RKR curve for the B state since our *ab initio* potential is close to it in the crossing region but the well depth is underestimated by roughly 10%. Note that our 2g potential has a minimum at long-range, $r_e = 7.1$ bohr, in contrast to the Buenker group potential, which is strictly repulsive. This causes the crossing to shift toward shorter distances and lower energies, which has important consequences for the effectiveness of the EP mechanism as a function of the vibrational quantum number. This point will be discussed in connection with the associated Franck–Condon factors in the next section.

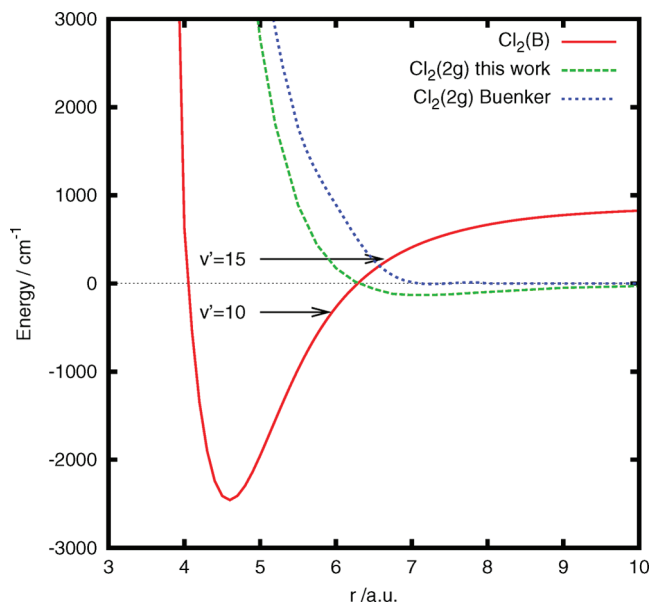


Figure 5. Potential energy curves for the Cl₂(B) and Cl₂(2g) states. For the B state the RKR potential of Coxon⁴⁶ was used. For the 2g state two curves are shown, one from Buenker and co-workers^{41,42} and one from this work. Note that our new potential shows a van der Waals well for large r , and crosses the B state potential at shorter r than does the Buenker group potential.

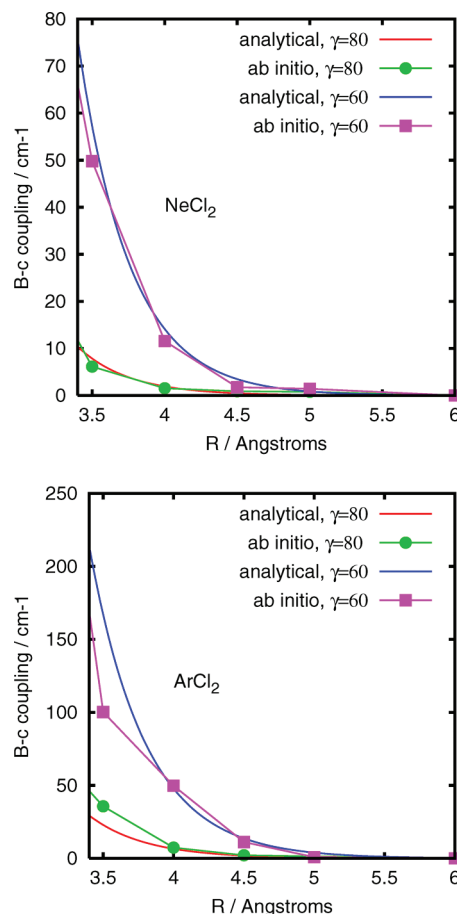


Figure 6. Estimated diabatic B-2g couplings from *ab initio* data and the fit using the functional form described in the text: Ne–Cl₂ (top panel) and Ar–Cl₂ (bottom panels).

To clarify the origin of this minimum and to obtain the best diatomic potential mentioned above, we performed all electron calculations on the ³Π_g state (main component of the 2g

spin–orbit state) using the extensive AVQZ basis set and three different methods for the treatment of electron correlation: MRCI, ACPF (averaged coupled pair approximation),⁴⁷ and CASPT2 (complete active space second order perturbation theory).⁴⁸ These calculations confirm the presence of a van der Waals minimum so that it is quite clear this is a real feature that is not present in the Buenker’s group potential. It is well-known that MRCI underestimates binding in weakly bound complexes due to limitations in the inclusion of higher order correlation, ACPF has a similar problem but improves on size consistency and CASPT2 may overestimate binding (see, for example, ref 49). As expected, the predicted binding energies are 119, 121, and 200 cm^{−1} for MRCI, ACPF, and CASPT2, respectively. We also calculated the ³Π_u state, which is the main component of the B state, to compare the *ab initio* methods with the accurate RKR potential available. The values for the dissociation energy are 2362, 3585, and 3338 cm^{−1} for ACPF, CASPT2, and RKR, respectively. The accurate prediction of the binding energy of the B state is a challenge for *ab initio* calculations (see, for example, refs 41 and 42), and given the good performance of the CASPT2 method, we decided to calculate the complete potential curve. We found that averaging the ACPF and CASPT2 results provides an excellent description of the B state, especially in the longer range part of the potential where the crossing of electronic states occurs. For this reason we decided to apply the same recipe in constructing our best estimate for the 2g potential to be used in the dynamics calculations and shown in Figure 5. The presence of the 2g minimum has important consequences on the EP predictions to be discussed below.

Although there are uncertainties in our *ab initio* estimations, the good agreement between calculated and measured quantities obtained using semiempirical PESs for the description of the VP dynamics for NeCl₂^{30,50} and ArCl₂¹⁵ indicate they are well suited for our study.

To simulate the EP dynamics of the NeCl₂ and ArCl₂ complexes, the corresponding 2g potential energy surfaces and couplings with the B state must be obtained. We have extended our previous³¹ RECP-MRCI calculations on a restricted grid: for the Cl₂ internuclear distance we cover mainly the region of the avoided crossing between the B and 2g states and up to the dissociation limit; for the angle we use the values 0, 30, 60, 80, and 90°, and for the intermolecular distance we cover the region of the van der Waals minima in the complex and up to the dissociation limit. Although the grid is not sufficient to obtain global representations of the surfaces, it is sufficient to characterize the crossing region and nonadiabatic couplings relevant for the EP process. To estimate the nonadiabatic couplings, we apply the following procedure: For fixed values of the angle we locate the avoided crossing region as a function of the internuclear and intermolecular distances. We find that the avoided crossing region occurs for a nearly constant value of the internuclear distance (6.1 bohr), but the magnitude varies as a function of the intermolecular distance. Using a 2 × 2 description of the adiabatic to diabatic transformation where the diagonal and off-diagonal elements are functions of the intermolecular distance, it is possible to obtain the coupling between diabatic states: $H_{12}(R)$. In this manner we obtain the coupling as a function of both the angle and the intermolecular distance. Note that the coupling between the B and 2g states is zero for the linear configuration since the angular momentum projection Ω becomes a good quantum number as in the case of the isolated diatomic halogen. This important point was overlooked in our previous study,³¹ the presence of a third

nearby electronic state complicated the adiabatic to diabatic transformation but has been taken into account in the coupling surfaces described below.

This information is then used to fit analytical representations as follows. For the 2g surface we use

$$V_{2g}(r, R, \gamma) = V_{2g}^{\text{Cl}_2}(r) + \sum_{i=1,2} D(e^{-2\alpha(R_i - R_e)} - 2e^{-\alpha(R_i - R_e)}) \quad (2)$$

where the first term corresponds to the new diatomic potential obtained for Cl₂(2g) but shifted to reproduce the experimental atomic spin–orbit splitting and the second term represents the van der Waals interactions as a sum of pairwise Morse functions (R_i is the distance between Rg and Cl atom i). The *ab initio* calculations performed on the complex suggests that there is a vdW well in the 2g electronic state, with similar features (equilibrium distance and well depth) as those of the B electronic state. Thus, the parameters used for the Ne(Ar)–Cl₂(2g) potentials are $D = 39$ cm^{−1}(106), $R_e = 4.2$ (4.5) Å, $\alpha = 1.8$ Å^{−1} for the Ne (Ar) complex.

The B-2g coupling is represented by

$$V_{B/2g}(r, R, \gamma) = \Delta e^{-\beta(R - \rho_e)} \sin \gamma \cos^2 \gamma \quad (3)$$

where the angular dependence is analogous to that obtained for ArI₂ using a DIM model.¹⁸ The dependence on R is as suggested by the *ab initio* calculations and the assumed constant dependence with r is consistent with a Landau–Zener type process.⁵¹ The values of the parameters are again obtained from fits to the *ab initio* calculations on the complex: $\Delta = 200$ cm^{−1} (600), $\rho_e = 3.6$ (3.6) Å, and $\beta = 2.8$ (2.5) Å^{−1} for the Ne (Ar) complex. In Figure 6 we show plots of the analytical couplings and the *ab initio* values for two angles. The plots show that the assumed functional form adequately represents the values deduced from the calculations. Note that the B/2g coupling is quite weak for $\gamma = 80^\circ$, 10° bent from the equilibrium geometry. For $\gamma = 60^\circ$, the coupling is significantly stronger. As might have been expected, for any given bent geometry, the coupling induced by Ar is stronger than that induced by Ne.

VIII. Role of Franck–Condon Factors

Franck–Condon factors often play an important role in the coupling between electronic states. If two states in different electronic manifolds have a significant Franck–Condon overlap, then it is expected that a perturbation due to a noble gas atom can induce coupling due to symmetry breaking or other intermolecular effects. In Figure 7 we present the Cl₂ (B, $v' = 15$ –17) bound vibrational wave functions and the Cl₂(2g) dissociative functions at the same energy, for both the Buenker group potential and the newly calculated potential. At the bottom of the figure the two sets of Franck–Condon factors are given for $v' = 10$ –28.

For the Buenker group 2g potential, the trend for the Franck–Condon factors as a function of the B state vibrational level is easy to visualize from the functions shown in Figure 7. The 2g potential is purely repulsive, so the inner turning point of the 2g dissociative wave functions gradually move toward small r as the energy increases. Similarly, the outer turning point of the B state functions move toward large r with increasing energy. The two functions start to overlap at $v' = 14$. For $v' = 16$ there is an interference because a complete wave of the 2g

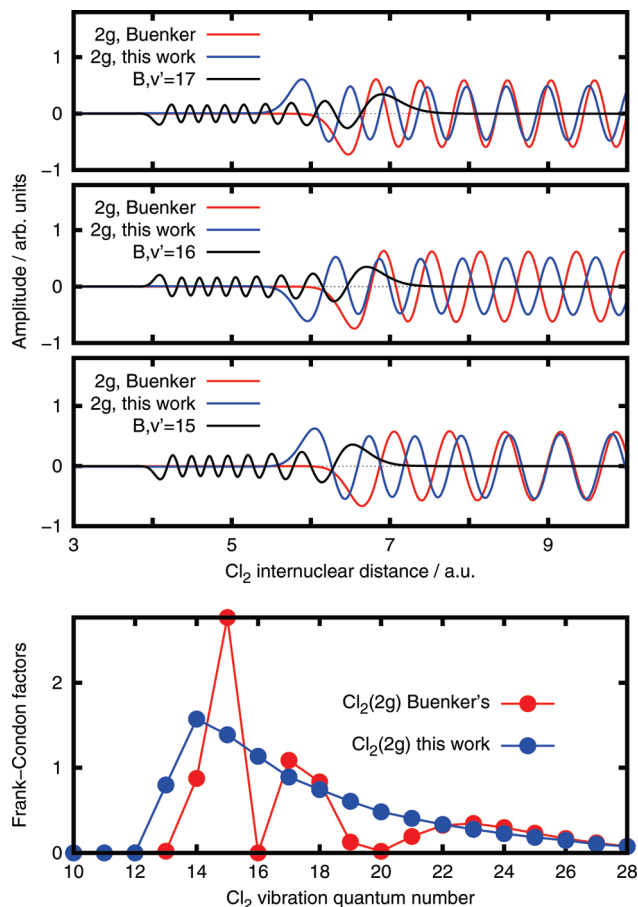


Figure 7. Franck–Condon factors (bottom panel) between the $\text{Cl}_2(\text{B}, v')$ vibrational state and the $\text{Cl}_2(2g, E=E_v)$ continuum states, whose potential curves are shown in Figure 5. The stretching vibrational wave functions used for $v' = 15, 16$, and 17 are displayed in the three top panels.

surface overlaps with the outer lobe of the B, $v' = 16$ function. The FC factors then increase again until the next such interference at $v' = 20$, and so on. So, for this potential one expects that the coupling between the B and 2g states may vary quite quickly with the B state vibrational level.

The FC factor trend for the newly calculated 2g state is quite different. The 2g potential is not purely repulsive, and even more important, the inner turning point is shifted toward shorter r and the slope of the potential is smaller at the crossing. So, the FC factors for this potential become finite for lower vibrational levels. Since the dissociative 2g eigenfunctions overlap with the bound $\text{Cl}_2(\text{B})$ function over a longer r interval, including several oscillations of the functions, the interferences disappear. The Franck–Condon factors increase between $v' = 12$ and $v' = 14$ and then decrease smoothly for higher v' values.

To the extent that FC factors play a prominent role in the coupling, these trends may help to determine the true shape of the 2g potential. We will show below that this process is not straightforward since the dependence of the coupling on the Franck–Condon factors is subtle, especially in the case of the newly calculated potential. For the Buenker group potential, it is clear that there will be little coupling below $v' = 14$, and one might expect to see an oscillatory pattern in the EP:VP ratio.

Finally, we comment on the uncertainty associated with the ab initio estimate for the crossing between the B and 2g states. With our current potential the crossing occurs at an energy corresponding to vibrational levels of the B state between $v' =$

12 and $v' = 13$. For the Buenker group strictly repulsive potential, the crossing is near $v' = 14$. As mentioned in section VII, there is strong evidence for the presence of a van der Waals minimum in the 2g potential and we are convinced that our potential provides a better estimate of the crossing position. It is clear that the pattern of Franck–Condon factors is very sensitive to the details of the potential. The relationship between Franck–Condon factors and the EP rate will be discussed further below. Next we study the competition between VP and EP for the two systems using a wave packet treatment.

IX. Theoretical Modeling of Electronic Predissociation

The potentials and couplings described above were employed in a three-dimensional wave packet calculation to study the competition between the EP and VP dynamics for NeCl_2 and ArCl_2 . Since the $\text{Cl}_2(2g)$ state is dissociative, the r coordinate cannot be represented in a basis of bound states as used above to study the VP in the isolated B state. The wave packet is therefore represented in a grid for the internal coordinates, r , R , γ and a basis set for the electronic states and Euler angles as

$$\Psi_t^{J,M,K} = \sqrt{\frac{2J+1}{8\pi^2}} \sum_{\Omega,e} D_{M\Omega}^{J*}(\phi, \theta, \chi) |e\rangle \Phi_{\Omega,e}^{J,K}(R, r, \gamma; t) \quad (4)$$

The initial wave packet is constructed for studying the VP dynamics in the so-called bright approximation, as described previously for ArI_2 .²⁴ The details of the computational method can be found in that reference and here only the required data are described. A two-dimensional grid of 256×160 points are used for the radial variables in the intervals $1.5 < r < 7 \text{ \AA}$, and $2.5 < R < 18 \text{ \AA}$. The angle γ is described by 35 Gauss–Legendre quadrature points in the interval $[0, \pi/2]$. A Chebyshev propagator is used, with a time interval of 20 fs up to, typically, several hundreds of picoseconds when the dissociation of the complexes is complete. After each time step, the wave packet is multiplied by an absorbing Gaussian for $r > 5 \text{ \AA}$ and $R > 15 \text{ \AA}$, with exponential constants of 0.05 and 0.025 for r and R , respectively. These propagations are computationally much more demanding than the studies described above for VP because many more components are required and the energy range is larger. So, more iterations are required for each time step, each of which is more expensive.

Using the proposed diabatic coupled potential energy surfaces model, the dissociation dynamics have been calculated for $\text{NeCl}_2(\text{B}, v')$ and $\text{ArCl}_2(\text{B}, v')$, $13 \leq v' \leq 21$ using both the Buenker group potential and the one proposed here to describe the 2g state. The results will be presented and discussed in the next section.

X. Results and Discussion

Figure 8 shows the final EP probability as a function of v' for the two dimers using each potential. As expected from the Franck–Condon analysis, the onset of EP occurs for higher v' levels for the Buenker group potential than for ours. The dependence of the EP probability on v' is quite different for the two molecules, showing that the influence of van der Waals interactions dominates that of the Cl_2 Franck–Condon factors.

Figure 9 shows the growth of the 2g population with time as calculated with the new potential proposed here. As v' increases, the growth stops at shorter times due to the completion of the VP dynamics. This is especially true for the higher levels of ArCl_2 for which the dissociation is complete after 3 ps. So, even

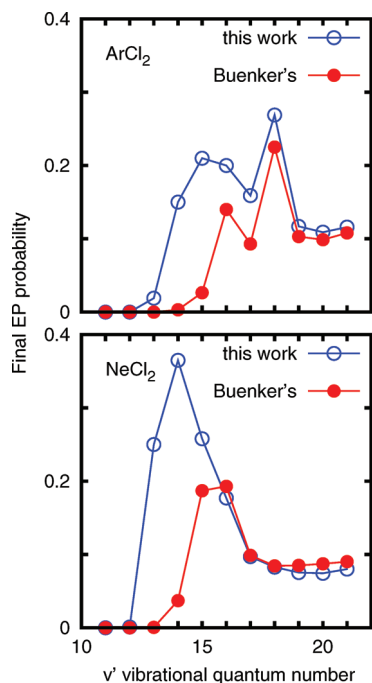


Figure 8. Final EP (electronic predissociation) probability for several initial states of NeCl₂(B,*v'*) and ArCl₂(B,*v'*) complexes.

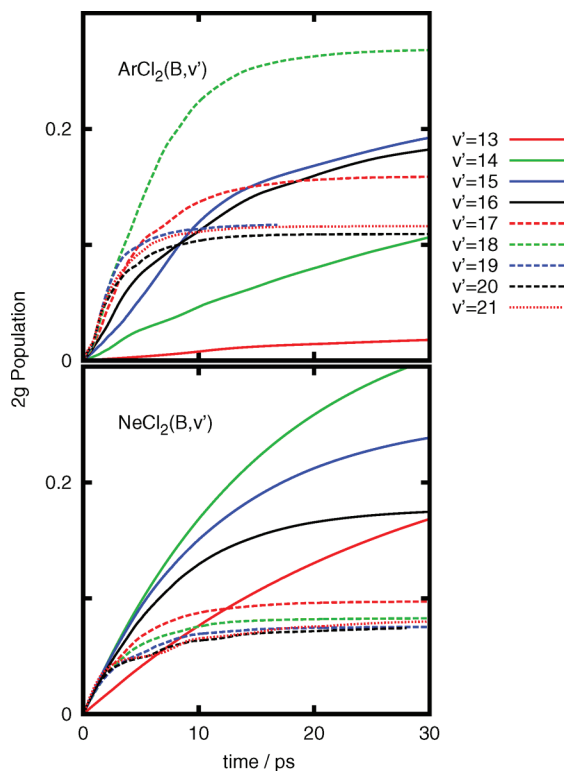


Figure 9. Population of the 2g electronic dark state versus time calculated with the new 2g potential for several initial states of the NeCl₂(B,*v'*) complex (bottom) and for ArCl₂(B,*v'*) top. The Cl₂(2g) potential calculated here has been used.

though the EP coupling is quite strong, VP still dominates. It is interesting to note that for the lower *v'* levels, EP is more important for NeCl₂ than ArCl₂, the opposite of the relative coupling strengths. Two effects may account for this apparent contradiction. For most of the vibrational levels, VP for ArCl₂ is faster than for NeCl₂. Also the coupling strength increases with bending, and the initial state bending amplitude is greater for NeCl₂ than for ArCl₂. Above *v'* = 14 the calculated EP

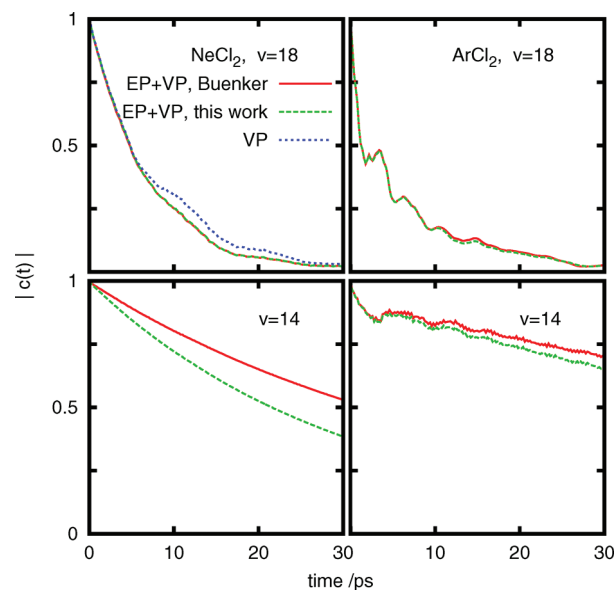


Figure 10. Autocorrelation function versus time for NeCl₂(B,*v*) (left) and ArCl₂(B,*v*) (right). Separate curves are shown for pure VP (blue, for NeCl₂(*v* = 18)), VP and EP calculated using the Buenker group 2g potential (red) and VP and EP calculated using the potential developed here (green).

contribution for NeCl₂ drops smoothly until it accounts for 8% of the decay for the highest levels of the calculation. For ArCl₂ the trend is not as smooth. The EP contribution is highest for *v'* = 18, 27%, then drops to 12% for *v'* = 19–21. Even though the initial state lifetime is only 3 ps for these levels, the EP contribution is still significant. Note that *v'* = 18 is the highest vibrational level that can decay with the loss of only two chlorine stretching quanta. This may account for its relatively long lifetime. The VP dynamics for the higher levels become especially fast as IVR enters the more statistical regime associated with $\Delta v' = -3$. It is also interesting to note that for these levels the EP contribution is greater for ArCl₂ than for NeCl₂, as would have been predicted from the B/2g coupling strength for the two molecules.

Greater detail is shown in Figure 10 for *v'* = 14 and 18. For NeCl₂ *v'* = 14, the initial state decay is smooth for both potentials. Since EP is quite small for the Buenker group potential, its curve overlaps that of pure VP. The new potential significantly speeds up the decay. For NeCl₂ *v'* = 18 EP has little effect for the first 5 ps, at which time a recurrence starts to appear in the pure VP curve. EP appears to retard the recurrence, leading to faster decay between *t* = 5 and *t* = 10 ps. That the EP rate increases just before the first recurrence of the IVR bright state, i.e., the initial state, suggests that EP is favored in the IVR dark state which is expected to involve wide amplitude bending.

Figure 10 also shows the initial state decay for ArCl₂ calculated for the two potentials for *v'* = 14 and 18. In neither case is the EP dynamics fast enough to quench the underlying VP recurrences. It is interesting to note that the overall decay rate is similar for the two molecules in *v'* = 18. This is the level for which EP is calculated to be most important for ArCl₂.

Next, we turn to the comparison with experiment. In the case of ArCl₂, an essential experimental observation for this paper is that the initial state decay is in the sparse IVR-VP regime for $8 \leq v' \leq 12$.^{22,52} This was determined by strong pump–probe signals that revealed complicated product rotational distributions. This has been analyzed previously by detailed theoretical calculations that are in qualitative agreement with the data. However,

in the IVR regime, the dynamics are so sensitive to the details of the potential that it appears to be impossible to achieve quantitative agreement between experiment and theory. Although the experimental pump–probe signals for $\nu' = 12$ were very strong, no signals at all could be observed for $\nu' = 13$. This was taken to be due to strong EP that leads to Cl_2 dissociation before the probe laser can detect molecular products. $\nu' = 13$ is the first Cl_2 B state vibrational level that is above the X state dissociation energy. The current calculations are in agreement with the data in the sense that the EP process contributes to the decay starting for $\nu' = 13$. However, the calculated EP rate is not fast enough to be consistent with the data. Given the difficulty of calculating the B/2g coupling strength, it seems quite possible that the new potential could be brought into agreement with experiment if the actual coupling strength is somewhat stronger than calculated here. It is clear that the Buenker group potential cannot account for the data in that the inner turning point of the 2g potential is at much too large r for EP to occur for $\nu' = 13$. In this regard, the new potential can be considered to be a substantial improvement, but not the final answer.

A very interesting result of the present calculation is the prediction that VP dynamics would again start to dominate EP for the higher vibrational levels. As VP enters the statistical regime, the VP lifetime falls below 3 ps. So, it would be very valuable to make an experimental search for VP products for the higher ArCl_2 levels. Similarly, it would be very valuable to search for EP products, presumably free Cl atoms, for $\nu' = 13$. These two observations would provide a strong confirmation of the results presented here.

The case of NeCl_2 is somewhat more puzzling. In this case, the calculated EP contribution is too large for low ν' , and too low for high ν' . The raw experimental data give no hint that EP occurs below $\nu' = 17$ and suggests that the EP process becomes important for $\nu' = 17$ –20. As discussed above, it is not out of the question that the NeCl_2 potential energy surface could be adjusted so that VP dynamics alone could account for the faster than expected loss of VP product signals for $\nu' \geq 17$. If the IVR–VP rate suddenly became extremely fast, with a broad range of $\Delta\nu'$, then the excitation band would become very broad and there would not be enough products in any one vibrational level to yield strong probe signals. However, the calculated VP rates are already somewhat faster than the experimental measurement for $14 < \nu' < 17$, and it is not obvious why the rate would be so much faster for $\nu' = 18$ and above.

Another possible way that the experiments and theory may be brought into accord is if another electronic state that crosses the B state curve at larger r values is responsible for the NeCl_2 EP dynamics. However, in our previous study of the Cl_2 excited state curves, no candidate for another effective EP state, crossing the B state at higher energy, was identified. Perhaps a more comprehensive search would identify one. A final possibility is that the EP dynamics for NeCl_2 are very sensitive to the details of the van der Waals interactions between the Ne atom and the 2g state. In this study we made a preliminary effort to calculate the van der Waals interactions, but this was not the focal point of the calculations. A particular difficulty of such calculations is that different methods are optimized for different aspects of the molecular properties. For instance, coupled cluster methods, which are well suited for obtaining van der Waals interactions are not applicable for excited states, especially far away from the equilibrium bond length. Since obtaining the perfect theory for NeCl_2 appears to be a formidable challenge, it would be very valuable to obtain more experimental data to guide the

search. Given the results presented here, it would be very valuable to search for chlorine atom products of EP dynamics as a function of excited state vibrational level. If such products can be observed for $\nu' = 13$ and 14, it would be a strong confirmation of the results presented here. If EP products are not observed for excitation to $\nu' = 17$, then we would know that future theoretical studies should concentrate on getting the best possible results for VP dynamics. On the other hand, if EP is observed to be much more important for $\nu' = 17$ than for $\nu' = 16$, as originally surmised from the data, then perhaps the theoretical search should concentrate on identifying a second possible electronic state to be involved in the EP. In any case, the results presented here confirm that the noble gas-halogen complexes provide a rich playground for exploring the competition between vibrational and electronic dynamics.

XI. Summary and Conclusions

We have reported new experimental data for NeCl_2 vibrational predissociation dynamics for the Cl_2 B state $16 \leq \nu' \leq 20$. The pump–probe signals for levels above $\nu' = 17$ are weaker than we had expected, and we initially concluded that this is due to the onset of electronic predissociation. Wave packet calculations for NeCl_2 vibrational predissociation for a previously determined potential energy surface are in excellent agreement with experimental data for $\nu' \leq 17$, suggesting that EP plays at most a minor role for these levels. The purely VP calculations do not fully account for the fall off of the experimental intensity for higher vibrational levels. However, for the potentials and couplings calculated here, EP also plays only a minor role for these higher levels. As discussed above, we postulate three explanations for this apparent disagreement between theory and experiment. First, another electronic state may be responsible for NeCl_2 EP for the higher vibrational levels. Second, subtle features of the van der Waals potential, not tested in the present calculations may play a more important role in the EP rate than expected. Finally, a more accurate potential than the one used here may show that VP dynamics alone may account for the experimental observations. In this regard, we note that the experimental data we are analyzing is negative in the sense that we see weaker VP pump–probe signals than expected for certain vibrational levels, but no search for EP products has been performed. Direct detection of EP products would be very valuable for a more complete understanding between the comparison of experiment and theory. In particular, it would be very valuable to detect electronic predissociation products for NeCl_2 $\nu' = 14$ and $\nu' = 17$. To obtain a more refined *ab initio* potential energy surface for low vibrational states, one can apply an analogous treatment to that of Valdes *et al.*^{53,54} For higher vibrational levels a combination of CI and CASPT2 methods as applied in this work for the chlorine molecule would help to determine the accuracy of the semiempirical model used here.

The results for ArCl_2 show better agreement between experiment and theory. The experimental observation was that VP products disappear for $\nu' \geq 12$. The calculations presented here with the improved 2g potential predict that the EP process turns on for $\nu' = 13$, in agreement with the data. However, for the experimental VP signal to disappear so completely will require that the B/2g coupling be somewhat larger than calculated here. The calculation of the B/2g coupling presented here is close to the current state-of-the-art. In this regard, obtaining satisfactory agreement between experiment and theory for this problem is an important test of current available methodology for electronic excited state problems that include spin–orbit coupling. One

possible direction for such work would be to calculate each of the electronic states and their couplings using the same level of theory. For ArCl₂, as for NeCl₂, direct measurements of the EP product yield as a function of v' would be very valuable. In particular, the calculations presented here suggest that VP products will be observed for ArCl₂, $v' \geq 19$, due to extremely fast IVR/VP. Confirmation of this result would be an important validation of this work.

Acknowledgment. This work has been supported by the US National Science Foundation Grant CHE-0404743, NSF-CONACYT J110.385 and the Ministerio de Ciencia e Innovación under projects CTQ2007-62898. R.H. and K.C.J. also acknowledge the UC-MEXUS program for aiding this collaboration.

References and Notes

- (1) Rohrbacher, A.; Williams, J.; Janda, K. C. *Phys. Chem. Chem. Phys.* **1999**, *1*, 5263.
- (2) Rohrbacher, A.; Halberstadt, N.; Janda, K. C. *Annu. Rev. Phys. Chem.* **2000**, *51*, 405.
- (3) Williams, J.; Rohrbacher, A.; Djahandideh, D.; Janda, K. C.; Jamka, A.; Tao, F. M.; Halberstadt, N. *Mol. Phys.* **1997**, *91*, 573.
- (4) Burke, M. L.; Klemperer, W. J. *Chem. Phys.* **1993**, *98*, 1797.
- (5) Janda, K. C.; Djahandideh, D.; Roncero, O.; Halberstadt, N. *Chem. Phys.* **1998**, *239*, 177.
- (6) Darr, J. P.; Glennon, J. J.; Loomis, R. A.; Herbert, J. M.; Ray, S. E.; McCoy, A. B. *J. Chem. Phys.* **2005**, *123*, 104312.
- (7) Pio, J.; van der Veer, W. E.; Bieler, C. R.; Janda, K. C. *J. Chem. Phys.* **2008**, *128*, 134311.
- (8) Miller, A. E. S.; Fu, C. C. H. C.; Higgins, K. F.; Klemperer, W. J. *Chem. Phys.* **1999**, *111*, 7844.
- (9) Williams, J.; Rohrbacher, A.; Seong, J.; Marianayagam, J. N.; Janda, K. C.; Burcl, R.; Szcześniak, M. M.; Chalasinski, G.; Cybulski, S. M.; Halberstadt, N. *J. Chem. Phys.* **1999**, *111*, 997.
- (10) Prosmi, R.; Villarreal, P.; Delgado-Barrio, G. *Chem. Phys. Lett.* **2002**, *359*, 473.
- (11) Valdés, A.; Prosmi, R.; Villarreal, P.; Delgado-Barrio, G. *Chem. Phys. Lett.* **2003**, *357*, 328.
- (12) Ray, S. E.; McCoy, A. B.; Glennon, J. J.; Darr, J. P.; Fesser, E. J.; Lancaster, J. R.; Loomis, R. A. *J. Chem. Phys.* **2006**, *125*, 164314.
- (13) Roncero, O.; Lepetit, B.; Beswick, J. A.; Halberstadt, N.; Buchachenko, A. A. *J. Chem. Phys.* **2001**, *115*, 6961.
- (14) Prosmi, R.; Cunha, C.; Buchachenko, A. A.; Villarreal, P.; Delgado-Barrio, G. *J. Chem. Phys.* **2002**, *117*, 10019.
- (15) Janda, K. C.; Roncero, O.; Halberstadt, N. *J. Chem. Phys.* **1996**, *105*, 5830.
- (16) Kubiak, G.; Fitch, P. S. H.; Wharton, L.; Levy, D. H. *J. Chem. Phys.* **1978**, *68*, 4477.
- (17) Johnson, K. E.; Sharfin, W.; Levy, D. H. *J. Chem. Phys.* **1981**, *74*, 163.
- (18) Buchachenko, A. A.; Halberstadt, N.; Lepetit, B.; Roncero, O. *Int. Rev. Phys. Chem.* **2003**, *22*, 153.
- (19) Burke, M. L.; Klemperer, W. J. *Chem. Phys.* **1993**, *98*, 6642.
- (20) Roncero, O.; Halberstadt, N.; Beswick, J. A. *J. Chem. Phys.* **1996**, *104*, 7554.
- (21) Roncero, O.; Gray, S. K. *J. Chem. Phys.* **1996**, *104*, 4999.
- (22) Roncero, O.; Caloto, D.; Janda, K. C.; Halberstadt, N. *J. Chem. Phys.* **1997**, *107*, 1406.
- (23) Lepetit, B.; Roncero, O.; Buchachenko, A. A.; Halberstadt, N. *J. Chem. Phys.* **2002**, *116*, 8367.
- (24) Roncero, O.; Buchachenko, A. A.; Lepetit, B. *J. Chem. Phys.* **2005**, *122*, 034303.
- (25) Breen, J. J.; Willberg, D. M.; Gutmann, M.; Zewail, A. H. *J. Chem. Phys.* **1990**, *93*, 9180.
- (26) Evard, D. D.; Bieler, C. R.; Cline, J. I.; Sivakumar, N.; Janda, K. C. *J. Chem. Phys.* **1988**, *89*, 2829.
- (27) Cline, J. I.; Sivakumar, N.; Evard, D. D.; Janda, K. C. *Phys. Rev. A* **1987**, *36*, 1944.
- (28) Cline, J. I.; Reid, B. P.; Evard, D. D.; Sivakumar, N.; Halberstadt, N.; Janda, K. C. *J. Chem. Phys.* **1988**, *89*, 3535.
- (29) Cline, J. I.; Sivakumar, N.; Evard, D. D.; Janda, K. C. *J. Chem. Phys.* **1987**, *86*, 1636.
- (30) Cline, J. I.; Sivakumar, N.; Evard, D. D.; Bieler, C. R.; Reid, B. P.; Halberstadt, N.; Hair, S. R.; Janda, K. C. *J. Chem. Phys.* **1989**, *90*, 2605.
- (31) Hernández-Lamoned, R.; Janda, K. C. *J. Chem. Phys.* **2005**, *123*, 161102.
- (32) Bieler, C. R.; Spence, K. E.; Janda, K. C. *J. Phys. Chem.* **1991**, *95*, 5058.
- (33) Bieler, C. R.; Janda, K. C. *J. Am. Chem. Soc.* **1990**, *112*, 2033.
- (34) Rohrbacher, A.; Janda, K. C.; Beneventi, L.; Casavecchia, P.; Volpi, G. G. *J. Chem. Phys.* **1997**, *101*, 6528.
- (35) Asano, Y.; Yabushita, S. *J. Phys. Chem. A* **2001**, *105*, 9873.
- (36) Cline, J. I.; Evard, D. D.; Reid, B. P.; Sivakumar, N.; Thommen, F.; Janda, K. C. In *Structure and dynamics of weakly bound molecular complexes*; Weber, A., Ed.; Reidel: Dordrecht, 1987; p 533.
- (37) Cabrera, J. A.; Bieler, C. R.; Olbricht, B. C.; van der Weer, W.; Janda, K. C. *J. Chem. Phys.* **2005**, *123*, 054311.
- (38) García-Vela, A.; Janda, K. C. *J. Chem. Phys.* **2006**, *124*, 034305.
- (39) Roncero, O.; Campos-Martínez, J.; Hernández, M. I.; Delgado-Barrio, G.; Villarreal, P.; Rubayo-Soneira, J. *J. Chem. Phys.* **2001**, *115*, 2566.
- (40) Tal-Ezer, H.; Kosloff, R. *J. Chem. Phys.* **1984**, *81*, 3967.
- (41) Kokh, D. B.; Alekseyev, A. B.; Bunker, R. J. *J. Chem. Phys.* **2001**, *115*, 9298.
- (42) Kokh, D. B.; Alekseyev, A. B.; Bunker, R. J. *J. Chem. Phys.* **2004**, *120*, 11549.
- (43) Chalasinski, G.; Szczeni, M. M. *Chem. Rev.* **2000**, *100*, 4227.
- (44) Bergner, A.; Dolg, M.; Kuechle, W.; Stoll, H.; Preuss, H. *Mol. Phys.* **1993**, *80*, 1431.
- (45) Werner, H.-J.; Knowles, P. J. MOLPRO, a package of *ab initio* programs, by Werner, H.-J.; Knowles, P. J. with contributions of Almlöf, J., Amos, R. D., Berning, A., Deegan, M. J. O., Eckert, F., Elbert, S. T., Hampel, C., Lindh, R., Meyer, W., Nicklass, A., Peterson, K., Pitzer, R., Stone, A. J., Taylor, P. R., Mura, M. E., Pulay, P., Schütz, M., Stoll, H., Thorsteinsson, T., Cooper, D. L., contributors; 2006.
- (46) Coxon, J. A. *J. Mol. Spectrosc.* **1980**, *82*, 265.
- (47) Gdanitz, R. J.; Ahlrichs, R. *Chem. Phys. Lett.* **1988**, *143*, 413.
- (48) Andersson, K.; Malmqvist, P. A.; Roos, B. O.; Sadlej, A. J.; Wolinski, K. *J. Phys. Chem.* **1990**, *94*, 5483.
- (49) Bartolomei, M.; Hernández, M. I.; Campos-Martínez, J.; Carmona-Novillo, E.; Hernández-Lamoned, R. *Phys. Chem. Chem. Phys.* **2008**, *10*, 5374.
- (50) Halberstadt, N.; Roncero, O.; Beswick, J. A. *Chem. Phys.* **1989**, *129*, 83.
- (51) Nakamura, H. In *Dynamics of molecules and chemical reactions*; Wyatt, R. E.; Zhang, J. Z. H. Eds.; Marcel Dekker: New York, 1996; p 473.
- (52) Halberstadt, N.; Serna, S.; Roncero, O.; Janda, K. C. *J. Chem. Phys.* **1992**, *97*, 341.
- (53) Valdés, A.; Prosmi, R.; Villarreal, P.; Delgado-Barrio, G.; Werner, H.-J. *J. Chem. Phys.* **2007**, *126*, 204301.
- (54) Valdés, A.; Prosmi, R.; Villarreal, P.; Delgado-Barrio, G.; Lemoine, D.; Lepetit, B. *J. Chem. Phys.* **2007**, *126*, 244314.
- (55) Evard, D. D.; Thommen, F.; Cline, J. I.; Janda, K. C. *J. Phys. Chem.* **1987**, *91*, 2508.

JP06392M